Technical University of Denmark

DTU

Electrochemical Deposition of Aluminum from NaCl-AlCl3 Melts

Li, Qingfeng; Hjuler, H. A.; Berg, Rolf W.; Bjerrum, Niels J.

DTU Library
Technical Information Center of Denmark

tributes nothing to $<S>$; Eq. [A-5] and [A-7] are unchanged (so is Eq. [15] in the text). However, $<1/S>$ becomes

$$<1/S> = \frac{1}{\lambda^2}\left[\frac{(1-\xi)}{\xi\sqrt{\xi^2 - \beta^2}} + \frac{1}{(2-\xi)}\right] \qquad [\text{A-14}]$$

which on combining with Eq. [A-7] yields Eq. [17].

LIST OF SYMBOLS

a interfacial area/total pore volume, cm^2/cm^3
b Tafel parameter, V
$\underline{c}(z)$ local concentration in micropore, mol/cm^3
$c(z)$ local concentration in macropore, mol/cm^3
C_1 integration constant, V/cm
D diffusivity, cm^2/s
F Faraday constant, C/eq
$i(z)$ interfacial current density, A/cm^2
i_0 exchange current density, A/cm^2
i_{avg} average interfacial current density, A/cm^2
$I'(z)$ total current along pore axis, A
L length of pore, cm
n electron number of reaction, eq/mol
n' number of spheres per unit area in Fig. 5, cm^{-2}
N number of constrictions per channel in constricted cubic pore structure
R Gas constant, $J/mol \cdot K$
$S(z)$ local cross-sectional area, cm^2
S_1 surface area scale in Eq. [1]-[3]
T temperature, K
z distance into pore from electrode-electrolyte interface, cm

Greek

α transfer coefficient, eq/mol
β dimensionless surface roughness size in Eq. [16] and [17]
Δ dimensionless average interfacial current density
ϵ_m macroscopic void volume fraction, dimensionless
ζ integration variable in Eq. [2], cm
η overpotential, V

κ electrolyte conductivity, $(\Omega\ cm)^{-1}$
λ local averaging distance, cm
ξ geometric parameter in Fig. 7, dimensionless
τ_c constriction factor, dimensionless
ϕ potential, V

REFERENCES

1. J. Euler and W. Nonenmacher, *Electrochim. Acta*, **2**, 268 (1960).
2. J. Newman and C. W. Tobias, *This Journal*, **109**, 1183 (1962).
3. K. Micka and I. Rousar, *Electrochim. Acta*, **25**, 1085 (1980).
4. K. Micka, *ibid.*, **27**, 765 (1982).
5. G. Wilemski, *This Journal*, **130**, 117 (1983).
6. J. Van Zee and R. E. White, *ibid.*, **130**, 2003 (1983).
7. E. Royaie and J. Jorne, *ibid.*, **131**, 1237 (1984).
8. K. C. Ho and J. Jorne, *ibid.*, **133**, 1394 (1986).
9. R. E. White, M. A. Nicholson, L. G. Kline, J. Van Zee, and R. Darby, *ibid.*, **131**, 268 (1984).
10. J. Newman and W. Tiedemann, *AIChE J.*, **21**, 25 (1975).
11. M. Kramer and M. Tomkiewicz, *This Journal*, **131**, 1283 (1984).
12. H. S. Lim, "Long Life Nickel Electrodes for Nickel-Hydrogen Cells," NASA CR-174815, p. 106ff (Dec. 1984).
13. P. Sides and C. W. Tobias, *This Journal*, **129**, 2715 (1982).
14. O. Lanzi and R. F. Savinell, *ibid.*, **130**, 799 (1983).
15. P. Fedkiw and J. Newman, *Chem. Eng. Sci.*, **33**, 1563 (1978).
16. K. Micka and M. Savata, *J. Power Sources*, **3**, 167 (1978).
17. T. Kessler and R. Alkire, *This Journal*, **123**, 990 (1976).
18. O. Lanzi and U. Landau, *ibid.*, **135**, 1922 (1988).
19. O. Lanzi and U. Landau, *ibid.*, **136**, 368 (1989).
20. M. Menon and U. Landau, *This Journal*, **134**, 2248 (1987).
21. G. W. D. Briggs, E. Jones, and W. F. K. Wynne-Jones, *Trans. Faraday Soc.*, **51**, 1433 (1983).
22. G. C. Akerlof and P. Bender, *J. Am. Chem. Soc.*, **70**, 2366 (1948).

Electrochemical Deposition of Aluminum from NaCl-AlCl₃ Melts

Li Qingfeng, H. A. Hjuler,* R .W. Berg, and N. J. Bjerrum

Molten Salts Group, Chemistry Department A, The Technical University of Denmark, DK-2800 Lyngby, Denmark

ABSTRACT

Electrochemical deposition of aluminum from NaAlCl₄ melts saturated with NaCl onto a glassy carbon electrode at 175°C has been studied by voltammetry, chronoamperometry, and constant current deposition. The deposition of aluminum was found to proceed via a nucleation/growth mechanism, and the nucleation process was found to be progressive. The morphology of aluminum deposits was examined with photomicroscopy. It was shown that depending on the current densities (c.d.) applied, three types of aluminum deposits could be obtained, namely, spongy deposits formed at lower c.d. (below 0.7 mA/cm²), smooth layers deposited at intermediate c.d. (between 2 and 10 mA/cm²), and dendritic or porous deposits obtained at high c.d. (above 15 mA/cm²). However, the smooth aluminum deposits were about five times more voluminous than the theoretical value. The spongy deposits were formed due to difficulties in electronucleation and could be inhibited by application of pulsed currents and/or addition of manganese chloride into the melt.

Aluminum has been used as anode material in newly developed rechargeable batteries with the NaAlCl₄ molten salt as the electrolyte and transition metal sulfides as cathodes at 175°C (1, 2). During the charging of the batteries, it was found (3) that aluminum dendrites can be formed under certain circumstances. The spacing between the electrodes in the batteries is usually very small; hence, the density of the deposits is of importance for the capacity and life of the batteries. Noncompact, dendritic deposits may cause short circuiting, early deterioration, and so on.

Barton and Bockris (4) and Diggle *et al.* (5) have developed a kinetic model of dendrite formation in which the role of a diffusion-controlled process was emphasized to account for the initiation and growth of dendrites. A set of rules governing the kinetics of dendrite formation was established, mainly that (*i*) a certain critical current density (overpotential) must be exceeded in order to provoke dendrite formation, (*ii*) dendrite growth exhibits a certain induction period before it becomes visible, and (*iii*) the critical current density or overpotential for dendrite formation is directly related to the concentration of the depositing species.

As early as the 1930s, aluminum dendrites were found to be favored during deposition at high current density from NaCl-AlCl₃ melts (6, 7). This was later studied by Midorikawa in a series of papers (8-10). Thereafter, several studies have been performed in this field (11-17). Many investigations supported the assumption of diffusion-controlled dendrite formation for aluminum deposition. As expected, a critical current density or overpotential is present for aluminum dendrite initiation, and the critical value is directly related to the mass transport conditions and the concen-

tration of species containing aluminum (12-14). Generally, in melts with less than 57 mole percent (m/o) $AlCl_3$, the critical current density is very small and dendrites are easily formed. This finding is unfortunate, since at high concentrations of $AlCl_3$ the melts are difficult to handle because of their high vapor pressures.

There were also reports suggesting that electrode substrates (8, 11, 15), inorganic and organic additives (10, 13, 16, 17), and superposed alternating current (8) or pulsed current (15) had significant effects on inhibiting aluminum dendrite formation. These findings cannot, of course, fit the mechanism of diffusion-controlled dendrite formation but suggest the governing role of the formation of crystalline nuclei in the deposition (14, 15). In the overvoltage measurement in a NaCl-KCl-$AlCl_3$ melt, Hayashi *et al.* (18) found that the main part of cathodic polarization seemed to be due to crystallization overvoltage in the low polarization potential region. Rolland and Mamantov (19) found that the reduction of $Al_2Cl_7^-$ in acidic chloroaluminate melts involved a nucleation process. Apart from this, little work has been done on the electrochemical nucleation and growth of aluminum from that medium. Moreover, almost all previous studies were performed in acidic NaCl-$AlCl_3$ melts, and little work has been reported in the basic NaCl-$AlCl_3$ melt saturated with NaCl. This system is of much more interest from the technical point of view because of its low vapor pressure. It was our intention to study the electrochemical nucleation process and to examine how and when the aluminum dendrites form in NaCl-saturated melts at 175°C.

Experimental

Preparation of chemicals.—Purification of $AlCl_3$ and NaCl and other experimental procedures have been previously described (3, 20). The equimolar NaCl-$AlCl_3$ melts, which were made from distilled $AlCl_3$ and analytic-grade NaCl dried at 200°C, became slightly yellow after several days of experimentation and some dark particles were always formed both on the aluminum electrode and in the melt. Further purification of the equimolar melts was therefore performed by zone refining carried out in a glass furnace consisting of nine stationary ring heaters. A certain amount of a mixture of 50.1 m/o distilled $AlCl_3$ and 49.9 m/o dried NaCl was charged into a Pyrex ampul of 200 mm length and 25 mm inner diameter. The ampul was then sealed off under vacuum and heated overnight in a rocking furnace. The heating zones of 35 mm width each were maintained at 158°C. The motion of the charged ampul involved a displacement range of 75 mm, which was repeated many times. The travel rate of the molten zones was 3 mm/h. The duration of the whole refining procedure was about 2 weeks.

After zone refining, the molten salts were colorless and allowed aluminum electrodes in the subsequent experiments to remain shiny and bright. However, a tiny amount of dark particles still appeared in the melt after some days of use.

Cell assembly and oven.—To facilitate the visual observation of the aluminum deposits, the cells were made of square Pyrex tubes. The working electrode was made of a glassy carbon rod (Type V10 from Le Carbone Lorraine) of 3 mm diameter (area 0.07 cm^2, as described earlier (3). Two aluminum rods of 99.999% purity joined to tungsten leads were used as the counter and reference electrode, respectively. The reference electrode was placed in the cell in such a way that it was surrounded mainly by $NaAlCl_4$ saturated with NaCl (*i.e.*, the composition of the melt before an experiment started). The test cell was placed into a transparent oven of our own construction, heated with circulated air. The aluminum deposits could be observed and photographed directly.

Instruments and measurements.—Voltammograms and potentiostatic current transients were obtained with an electrochemical system built in this laboratory (21) and recorded on a Hewlett-Packard X-Y recorder (Type 7004B). After each set of measurements, the working electrode was kept at a positive potential of 100 mV *vs.* aluminum for

at least half an hour and then left for another half hour to eliminate the concentration polarizations.

Aluminum deposits were achieved by electrolysis at constant current, which was delivered by a chronoamperostat built in this laboratory. To ensure that sufficient metal was deposited to provide a visible layer of aluminum deposits, a total charge of *ca.* 30 C/cm^2 was employed in each run, corresponding theoretically to a 0.01 mm thickness of uniformly plated aluminum. The duration of each deposition experiment varied from several minutes to more than 20h, depending on the current density applied. After deposition, the aluminum deposits were observed by using a Zeiss Jena Technival 2 Stereo Microscope equipped with an Olympus OM-2 SLR camera and a Schott KL 1500 cold light source. The morphology of the aluminum deposits was examined by microphotography and the specific volume of the smooth deposits was measured as averages from the pictures.

Results and Discussion

Voltammograms.—Figure 1 shows voltammograms obtained in both slightly acidic (Fig. 1a) and slightly basic (saturated with NaCl, Fig. 1b) NaCl-$AlCl_3$ melts at 175°C. The small current peak A in Fig. 1a may be attributed to the $Al_2Cl_7^-$ reduction which starts at *ca.* −50 mV *vs.* the aluminum reference. Rolland and Mamantov (19) found the same overpotential value in their electrochemical study. The peak was followed by the $AlCl_4^-$ reduction. In the voltammogram from the basic melts (Fig. 1b), the current peak disappeared. In this case only $AlCl_4^-$ reduction occurred starting at *ca.* −65 mV *vs.* aluminum. In the cathodic branches of both voltammograms, cross-over loops appeared on reversing sweeps characterizing the presence of a nucleation/growth process. Integration of both the cathodic and the anodic currents of the voltammograms obtained from the basic melts gave a charge ratio, Q_c/Q_a, between 1.01-1.05, indicating that the reduction of $AlCl_4^-$ behaves reversibly in a chemical sense.

Chronoamperograms.—Figure 2 shows a set of potentiostatic current-time transients obtained at different overpotentials in $NaAlCl_4$ saturated with NaCl. For all overpotentials applied, there appears to be a peak current transient corresponding to the charging of the electric double layer. For overpotentials below 65 mV *vs.* the Al reference, there is no reduction current. A nucleation overpotential of at least 65 mV is required for any significant electrodeposition to take place. This is in agreement with the overpotential observed in voltammetric measurement for the same electrode and the same NaCl-saturated melt. For overpotentials larger than 70 mV, the capacitive charging current was followed by a rising current due to the formation of new nuclei. As the nuclei grew, the overlap of nuclei or neighboring diffusion zones gave rise to a current maximum followed by a falling portion of current. The time to reach the maximum current decreased as the applied overpotentials increased (Fig. 2a).
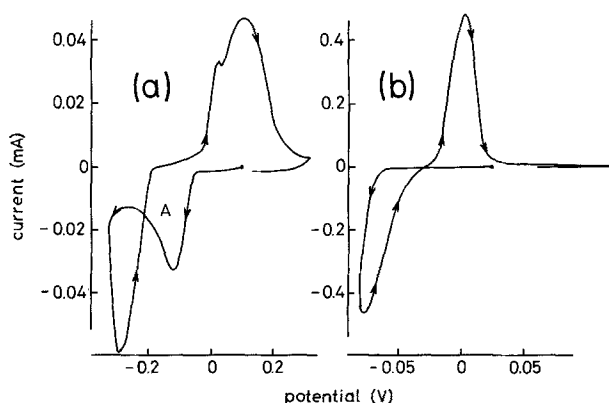
Fig. 1. Voltammograms on glassy carbon electrodes at 175°C; sweep rates were 10 mV s⁻¹. (a) 49.7 m/o NaCl-50.3 m/o $AlCl_3$ melt. (b) $NaAlCl_4$ saturated with NaCl.
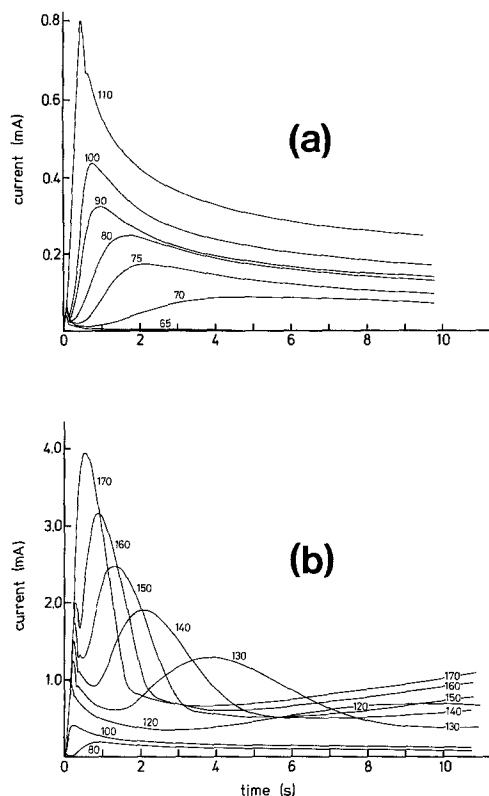
Fig. 2. Potentiostatic current transients for deposition of aluminum onto a glassy carbon electrode (3 mm diam) from a NaCl-saturated melt (a) at low overpotentials (mV), and (b) at high overpotentials (mV). Applied overpotentials (mV) vs. aluminum reference are indicated in the figure. For clarity not all measured current transients are shown. Electrode area, 0.07 cm², temperature, 175°C.

When large overpotentials are applied, the time required to reach the maximum current becomes so short that the capacitive current peak is not distinguishable from the rising portion of the current transients due to the faradaic process. After the first maximum in the transients, the current rises again, and a second current maximum appears thereafter when overpotentials larger than 120 mV are applied (Fig. 2b). As nucleation proceeds continuously, new nuclei are formed on top of the first deposited layer long before it has covered the whole area of the electrode surface, i.e., multinuclear multilayer growth occurs (22).

For a three-dimensional nucleation, expressions for the theoretical current transients describing both the rising and the falling parts have been obtained for both instantaneous and progressive nucleations (23, 24). A convenient criterion for distinguishing between the two mechanisms is to represent the experimental data in the dimensionless plot, $(i/i_m)^2$ vs. t/t_m, where i_m and t_m are the coordinates of the current maximum on the current transients. This analysis can be made by comparing the experimental data with theoretical plots resulting from Eq. [1] and [2] for instantaneous and progressive nucleations, respectively (24)

$$(i/i_m)^2 = 1.9542\ (t/t_m)^{(-1)}\ \{1 - \exp\left[-1.2564\ (t/t_m)\right]\}^2 \quad [1]$$

$$(i/i_m)^2 = 1.2254\ (t/t_m)^{(-1)}\ \{1 - \exp\left[-2.3367\ (t/t_m)^2\right]\}^2 \quad [2]$$

It is found that the dimensionless plot of our experimental data fits to the theoretical curve corresponding to progressive nucleation except for low values of t/t_m. As demonstrated (25), the experimental current transients are affected by a certain time delay, t_o. The exact comparison is possible only after correction of the time scale by defining

$$t_{\text{real}} = t - t_o \quad [3]$$

Figure 3 shows the graphical analysis of the rising portion of current transients. A linear dependence of $i^{2/3}$ on time is found, indicating the progressive nature of the nucleation process as required by the following equation (25)

$$i = \frac{2}{3}\ zF\pi\ (2Dc)^{(3/2)}\ (M/\rho)^{(1/2)}\ N_t^{(3/2)} \quad [4]$$

Here zF is the molar charge of the deposited species, D is its diffusion coefficient, c is its concentration in mol cm^{-3}, M is its molecular weight, and ρ is the density of the electrolyte. This is in accordance with the conclusion obtained from the dimensionless analysis. The straight lines of $i^{2/3}$ vs. t intercept the time axis at $t_{\text{real}} = t - t_o = 0$, i.e., $t = t_o$. Therefore, the delay time, t_o, needed for the time correction can be obtained. After correction of the time scale with t_o obtained this way, the dimensionless plot of the experimental data is well superimposed on the theoretical curve, corresponding to a progressive nucleation process (Eq. [2]), as shown in Fig. 4.

Aluminum dendrite formation.—Aluminum deposits obtained by electrochemical reduction from NaAlCl$_4$ melt saturated with NaCl can vary greatly in their outer appearance depending on the depositing conditions. They can be smooth, rough, dendritic, or porous as the current densities increase. Several types of surface morphology of alu-
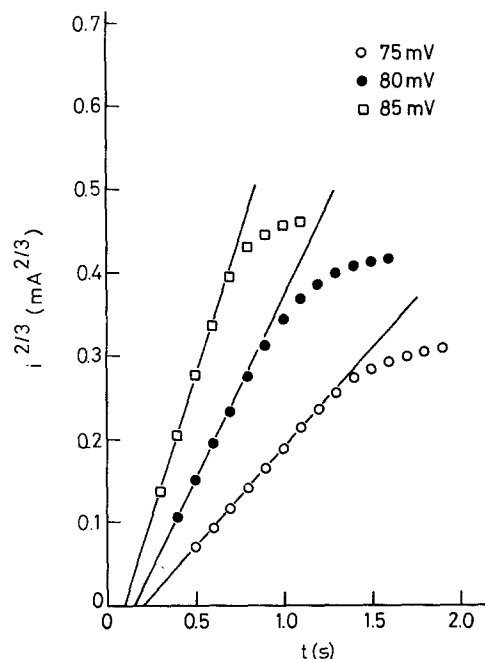

Fig. 3. Plots of $i^{2/3}$ vs. time for the rising portions of some current transients. Overpotentials indicated in the figure.
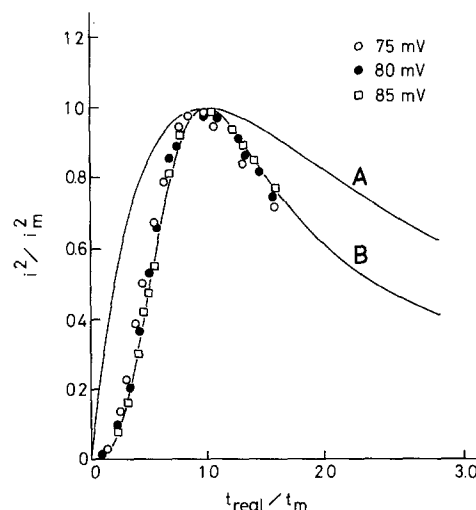

Fig. 4. Dimensionless plots for overpotentials of 75, 80, and 85 mV with time correction. Theoretical curves (A) for instantaneous and (B) for progressive nucleation.
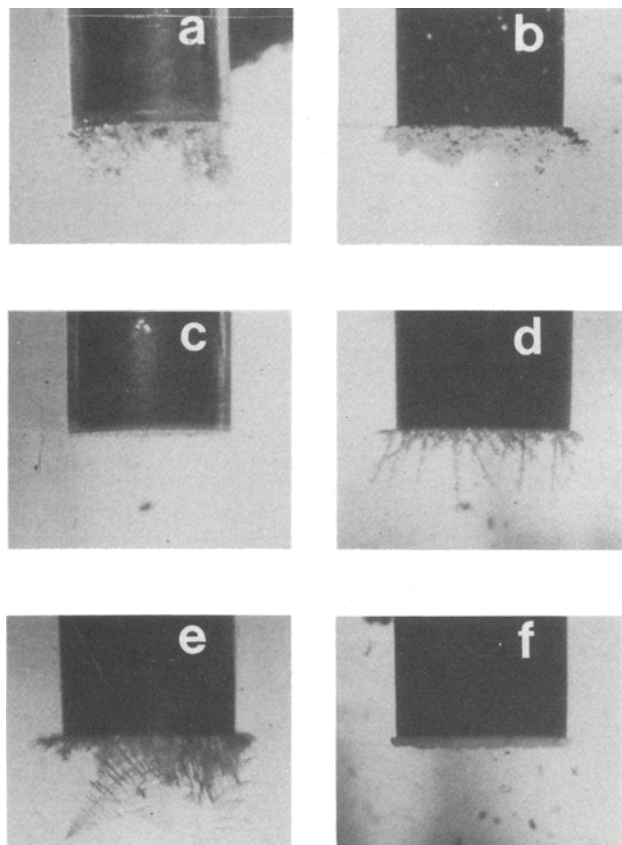
Fig. 5. Different types of aluminum deposits obtained from constant current deposition on a glassy carbon electrode (3 mm diam) in NaAlCl$_4$ saturated with NaCl at 175°C. (a) Spongy deposits, 0.43 mA/cm^2, 18.5h. (b) Spongy deposits, 0.57 mA/cm^2, 14h. (c) Smooth deposits, 4.3 mA/cm^2, 1.85h. (d) Needle-like deposits, 21 mA/cm^2, 22 min. (e) Fir-tree-like dendrites, 28 mA/cm^2, 17 min. (f) Porous deposits, 43 mA/cm^2, 8 min.

Fig. 6. Aluminum deposits on a glassy carbon electrode of 3 mm diam at 175°C. (a) Constant current, 0.285 mA/cm^2, 3.5h, NaAlCl$_4$ saturated with NaCl. (b) Constant current, 1.14 mA/cm^2, 6.95h, NaAlCl$_4$ saturated with NaCl. (c) Pulsed current, 1.14 mA/cm^2 (i_d/A) (A = electrode area), 6.95h, NaAlCl$_4$ saturated with NaCl. (d) Constant current, 1.14 mA/cm^2, 6.95h, NaAlCl$_4$ saturated with both NaCl and MnCl$_2$.

minum deposits are shown in Fig. 5. In the NaAlCl$_4$ melt saturated with NaCl at 175°C, it seems that spongy deposits are always formed at low current densities ($< ca.$ 0.7 mA/cm^2, see Fig. 5a and b); at intermediate ranges of current densities between 2 and 10 mA/cm^2, aluminum deposits appear smooth and granular (Fig. 5c), while at very high current densities ($> ca.$ 15 mA/cm^2) needle-like or fir-tree-like dendrites or very porous deposits are often obtained (Fig. 5d, e, and f).

Aluminum grains formed during deposition can easily be observed with a microscope by using grazing illumination. It is found that the grain size of the aluminum deposits decreases as the current density increases. At a very low current density (0.285 mA/cm^2), separated aluminum particles can be obtained on the electrode surface as shown in Fig. 6a, and in this case the spongy aluminum deposits will form after prolonged deposition. Aluminum particles show a great variety of sizes, which confirms the progressive character of the nucleation process.

It is known from the electrocrystallization theory (26) that the grain size is determined primarily by the number of nuclei formed during the deposition process. The formation of the spongy deposits at lower current density can thus be attributed to the lack of nuclei originally formed serving as growth centers. It was known that aluminum deposition from NaCl-AlCl$_3$ molten salts proceeds via a nucleation/growth mechanism. The difficulty in electronucleation of aluminum deposits is thus assumed to be the cause of formation of spongy deposits at low current density.

A critical thickness of aluminum deposits, as well as the variation of aluminum grain sizes with current density of deposition, was also observed in an aluminum electroplating study (14). The assumption of the predominant role of the electronucleation of aluminum in the deposition pro-
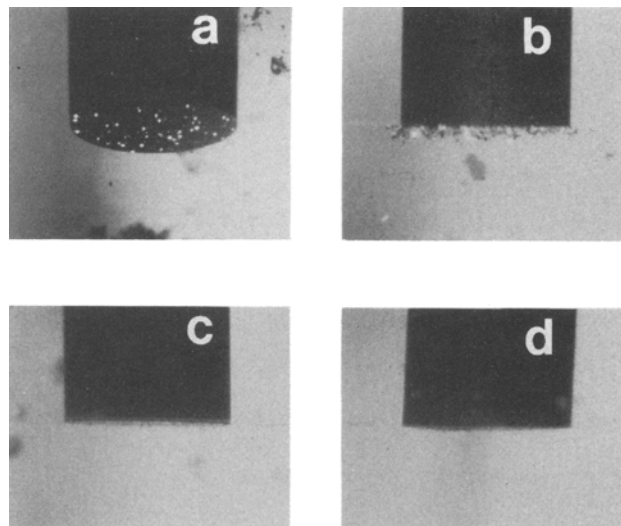
cess was also supported by the high effect of organic surfactants (13, 14, 16, 17) such as tetramethylammonium chloride (TMA) and urea. The organic surfactants were supposed to block the active sites on the cathode surface and result in an energetic homogenization of the surface and consequently lead to an increased number of growing nuclei.

With an increase in current density (overpotential), the electronucleation process becomes faster and more precursory nuclei can be formed during the deposition process. The formation of the spongy deposits will thus be suppressed during the subsequent growth. Smooth aluminum deposits can thus be formed when deposition is done at intermediate current densities.

At high current density, the whole deposition process is brought under the control of slow transport of depositing ions from the bulk to the electrode surface. In this case, aluminum dendrites as previously discussed (4, 5) are formed. The much faster growth of a dendritic aluminum protrusion relative to aluminum on the rest of the electrode surface lies mainly in the different diffusion conditions, $i.e.$, that spherical diffusion occurs around the dendritic tips whereas linear diffusion prevails elsewhere. The concentration gradient of species containing aluminum resulting from electrolysis may also drive the excessive growth of aluminum dendrites as proposed in our previous study (3).

A characteristic of diffusion-controlled dendrite formation is the critical current density or overpotential for the initial dendrite formation (12-14). The values of critical current densities are directly related to the composition of the melt. For the NaAlCl$_4$ melt saturated with NaCl, the irregular dendrites or porous deposits were often obtained when current densities exceeding 15 mA/cm^2 were applied to a glassy carbon electrode. Grjotheim and Matiašovský (13) found that at current densities up to 50 mA/cm^2 aluminum was deposited in the form of a fine crystalline layer on a steel substrate from an electrolyte containing 63.6 m/o AlCl$_3$. Fellner et al. (14) observed a similar critical value on iron cathodes in a ternary NaCl-KCl-AlCl$_3$ system containing 56.8-63.6 m/o AlCl$_3$. Smith et al. (27, 28) found that the critical current density decreased dramatically to $ca.$ 1 mA/cm^2 in the ternary AlCl$_3$-based melts containing $ca.$ 50 m/o AlCl$_3$.

All of the results cited were obtained by using iron or steel substrates. Therefore the difference in critical current densities between the cited literatures and ours may be partly attributed to the different composition of the melt and to the different electrode substrates used. Moreover,

Nayak *et al.* (11) found that electrodeposition of aluminum on brass from 36.4 m/o NaCl-63.6 m/o $AlCl_3$ led to nondendritic crystal deposits at current densities of up to 53 mA/cm². Pretreatment of a mild steel substrate by electropolishing in the electrolyte itself was also found to be very helpful in eliminating dendrite formation (12). The fact that the substrates have such a pronounced effect on aluminum deposition also suggests the importance of the nucleation process. It seems correct to say that even in the case of diffusion-controlled dendrite formation, the electronucleation process may play a certain role in dendrite formation.

The smooth aluminum deposits obtained at intermediate current densities between *ca.* 2 and 10 mA/cm² are not compact. Figure 7 shows the results of the average volume of the aluminum deposits per coulomb *vs.* the current density that was applied. The volumes were all measured on photographs of the deposits. The deposits obtained from $NaAlCl_4$ saturated with NaCl by constant current deposition look porous. The values for the volume of aluminum are about five times or more larger than the theoretical value of 0.0345 mm³/C for a compact layer of aluminum. The larger values obtained at low and high current densities during constant current deposition reflect the formation of two types of deposits, *viz.*, the electronucleation-controlled formation of spongy deposits at low current densities and the diffusion-controlled formation of dendrites at high current densities.

It seems of importance to distinguish the two mechanisms from one another. Consequently, different techniques may be used to inhibit the formation of individual kinds of dendrites. For instance, to avoid dendritic formation caused by the slow nucleation process at low current density, a pulsed current shown in Fig. 8 was used. A single pulse of current (i_p) ten times as large as the deposition current (i_d) and with a duration of 10s was applied at the beginning of the experiment in order to accelerate the nucleation process. A small deposition current (i_d) was then used to avoid the dendrite formation caused by the diffusion-controlled process afterward. In this way, the spongy deposits can be completely eliminated. The volume of the aluminum deposits obtained by the pulsed current deposition is also shown in Fig. 7. It can be seen that the compactness of the aluminum deposits was much improved by this pulse technique, especially at low current densities. Apparent differences between aluminum deposits obtained at the same deposition current density (1.14 mA/cm²) with and without the initial current pulse are shown in Fig. 6b and c. Furthermore, the addition of manganese chloride into the melt can also significantly improve the quality of deposits, as seen in Fig. 6d. Detailed studies are now under way to explore the effect of manganese chloride addition on aluminum deposition.
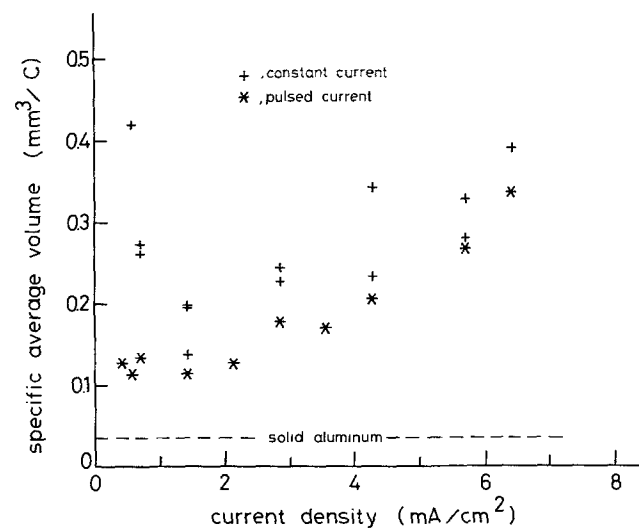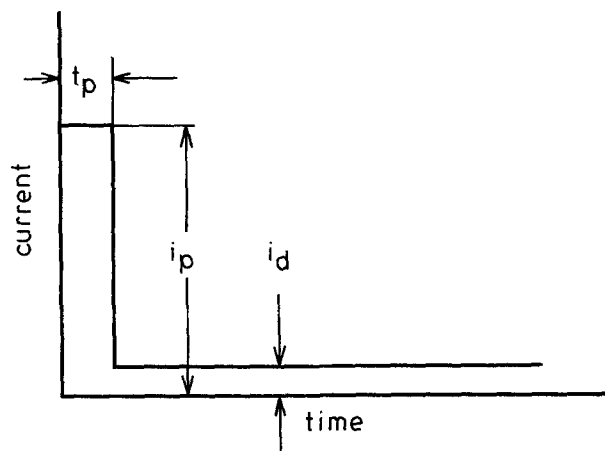

Fig. 8. Pulsed current diagram: i_p, initial current pulse, t_p, duration of current pulse, and i_d, deposition current. t_p is always 10s, i_p is always ten times as large as i_d, and i_d continued until a total charge of *ca.* 30 C/cm² has been transferred.

Conclusions

Electrochemical deposition of aluminum onto glassy carbon electrodes from $NaAlCl_4$ saturated with NaCl at 175°C has been investigated and found to proceed via a nucleation/growth mechanism. The nucleation process was found to be progressive. Several types of aluminum deposits can be electrodeposited from the melt, mainly depending on the current densities applied. It is observed that only at intermediate current densities, between 2 and 10 mA/cm², can a smooth layer of aluminum be formed. The smooth deposits are still about five times more voluminous than the theoretical value. At high current densities, above *ca.* 15 mA/cm², needle-like or fir-tree-like dendrites or very porous deposits were often obtained. The deposits were attributable to the slow diffusion process of species containing aluminum. At lower current densities, below *ca.* 0.7 mA/cm², aluminum was deposited in the form of spongy deposits, apparently due to the slow nucleation process. The spongy deposits can be inhibited by using pulsed current deposition or by adding manganese chloride to the melt.

REFERENCES

1. H. A. Hjuler, R. W. Berg, and N. J. Bjerrum, *Power Sources*, **10**, 1 (1985).
2. N. Takami and N. Koura, *Denki Kagaku*, **54**, 498 (1986).
3. Li Qingfeng, H. A. Hjuler, R. W. Berg, and N. J. Bjerrum, *This Journal*, **136**, 2940 (1989).
4. J. L. Barton and J. O'M. Bockris, *Proc. R. Soc. London*, **A268**, 485 (1962).
5. J. W. Diggle, A. R. Despic, and J. O'M. Bockris, *This Journal*, **116**, 1503 (1969).
6. K. M. Gorbunova and Tz. A. Adzhemyan, *Comp. Rend. Acad. Sci. U.S.S.R.*, **1**, 564 (1934).
7. J. Czochralsky and J. Mikolajczyk, *Wiadomosci Inst. Metalurg. Metaloz.*, **15**, 58 (1938).
8. R. Midorikawa, *Denki Kagaku*, **24**, 366 (1956).
9. R. Midorikawa, *ibid.*, **24**, 511 (1956).
10. R. Midorikawa, *ibid.*, **24**, 562 (1956).
11. B. Nayak and M. M. Misra, *J. Appl. Electrochem.*, **7**, 45 (1977).
12. B. Nayak and M. M. Misra, *ibid.*, **9**, 699 (1979).
13. K. Grjotheim and K. Matiašovský, *Acta. Chem. Scand.*, **A34**, 666 (1980).
14. P. Fellner, M. Chrenková-Paučirová, and K. Matiašovský, *Surf. Technol.*, **14**, 101 (1981).
15. M. Chrenková-Paučirová, P. Fellner, A. Silný, and K. Matiašovský, *ibid.*, **16**, 15 (1982).

Fig. 7. Specific average volume of smooth layer of aluminum deposits, in mm³ per coulomb, on a glassy carbon electrode in $NaAlCl_4$ saturated with NaCl as function of current density.

16. Y. K. Delimarsky and N. K. Tumanova, *Electrochim. Acta.*, **24**, 19 (1979).
17. M. Paučírová and K. Matiašovský, *Electrodep. Surf. Treat.*, **3**, 121 (1975).
18. T. Hayashi, Y. Kuwa, M. Yoshida, and N. Kikumoto, *Denki Kagaku*, **33**, 584 (1965).
19. P. Rolland and G. Mamantov, *This Journal*, **123**, 1299 (1976).
20. R. W. Berg, H. A. Hjuler, and N. J. Bjerrum, *Inorg. Chem.*, **23**, 557 (1984).
21. F. W. Poulsen and N. J. Bjerrum, *J. Electroanal. Chem.*, **79**, 327 (1977).
22. R. D. Armstrong and J. A. Harrison, *This Journal*, **116**,

23. 328 (1969).
23. G. Gunawardena, G. Hills, I. Montenegro, and B. Scharifker, *J. Electroanal. Chem.*, **138**, 225 (1982).
24. B. Scharifker and G. Hills, *Electrochim. Acta*, **28**, 879 (1983).
25. P. M. Rigano, C. Mayer, and T. Chierchie, *J. Electroanal. Chem.*, **248**, 219 (1988).
26. R. Greef, R. Peat, L. M. Peter, D. Pletcher, and J. Robinson, "Instrumental Methods in Electrochemistry," Chap. 9, p. 283, Halsted Press, New York (1985).
27. E. J. Smith, M. G. Vucich, and L. W. Austin, U.S. Pat. 3,226,315 (1965).
28. E. J. Smith and L. W. Austin, U.S. Pat. 3,267,008 (1966).

Analysis of the Response of Ion Sensing FETs with a Chemically Modified Gate Insulator

Hubert Perrot, Nicole Jaffrezic-Renault, and Paul Clechet*

Laboratoire de Physico-chimie des Interfaces, URA CNRS 404, Ecole Centrale de Lyon-BP 163, 69131 Ecully Cedex, France

ABSTRACT

This paper is devoted to the analysis of the physicochemical parameters influencing the response of ion sensing FETs obtained by chemical grafting of the silica gate insulator. The site binding theory has been applied to the modified silica/electrolyte interface; for the first time the equilibria involving H^+ and M^+ ions have been taken into account. The established theoretical expression ψ_o-pM shows that the sensitivity of the ion sensing FETs is better when the number of sensitive sites and the complexation constant of these sites are higher. The experimental response of the Ag^+ sensing ISFET was fitted with this model. The percentage of cyanografted sites is determined to be 8%; their complexation constant is −0.9.

ISFET-type chemical sensors consist of an insulated gate field effect transistor (IGFET) where the metallic gate is replaced by a sensitive membrane, an electrolyte, and a reference electrode. At the interface between the insulator and the solution, the electric potential difference depends on the composition of the solution (pH or other ions) and on the nature of the insulator surface. Several dielectrics were used for pH detection: SiO_2 (1), Si_3N_4 (2), Al_2O_3 and Ta_2O_5 (3). For ion detection the dielectric surface was modified by adding several types of specific membrane to the insulator surface: special glass for Na^+ and K^+ detection (4), insoluble salts for halogenide detection, polymeric membranes with inserted ionophore groups for detection of K^+, Na^+, Ca^{2+} (5), NO_3^- (6), Cl^- (7) ions. Ion specificity was also conferred onto the directly modified insulator surface by ion implantation (8) for Na^+ detection or by chemical grafting. The feasibility of an Ag^+ sensing ISFET through chemical grafting of the silica surface with cyanopropylsilane has been shown (9, 10). The devices obtained have a long lifetime (11) and a short response time (9). This paper is devoted to the analysis of the parameters influencing the ion response of this type of device.

The potential/pH response of the oxide membrane ISFET is based on the acid/base behavior of hydroxyl groups on the surface. The site binding theory which was first applied to pH sensitive ISFET by Siu and Cobbold (12) allows the fit of the response of the ISFETs by introducing a sensitivity constant β (13, 14). Very recently, the site binding theory was extended to a dielectric surface with two types of sites: the Si_3N_4 membrane with amphoteric hydroxyl groups and the basic amine groups (15). For both sites the potential determining ion is H^+. In this paper, we present the site binding theory for a modified insulator surface: a silica ISFET grafted with ionophore groups which presents a specific response for ions different from H^+, the remaining amphoteric hydroxyl groups being pH sensitive. This model is applied to the cyanografted silica membrane; the potential determining ions are Ag^+ and H^+ (9-11).
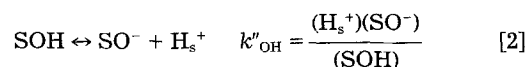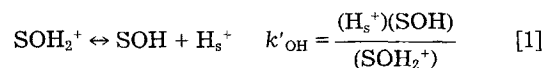
* Electrochemical Society Active Member.

Site Binding Theory Applied to Grafted Silica Surface

Surface reactions.—The two types of sites on the grafted silica surface are amphoteric hydroxyl sites, called SOH, and the ionophore grafted sites called S-X.

It is assumed that no surface complexation of M^+ occurs with hydroxyl groups, as has been observed in the case of Ag^+ ions, the flatband potential of Si/bare SiO_2/electrolyte only being slightly shifted in the presence of Ag^+ ions (10). The S-X sites are assumed to present no amphoteric properties as has been shown through the electrokinetic properties of CN-grafted silica in colloidal aqueous suspensions (16). Thus, each type of site reacts with one specific ion: H^+ with the amphoteric SOH sites and M^+ with the S-X sites. The formation of surface complexes between charged surface sites (SOH_2^+ and SO^-) and counterions in the solution will be neglected. Such surface complexes have been shown to have a negligible effect on the surface potential (14).

The equations describing the surface reactions of the two sites are:

Amphoteric reactions of SOH.—

$$SOH_2^+ \leftrightarrow SOH + H_s^+ \qquad k'_{OH} = \frac{(H_s^+)(SOH)}{(SOH_2^+)} \qquad [1]$$

$$SOH \leftrightarrow SO^- + H_s^+ \qquad k''_{OH} = \frac{(H_s^+)(SO^-)}{(SOH)} \qquad [2]$$

Surface complexation of M^+ with S-X sites.—

$$S\text{-}X + M_s^+ \leftrightarrow S\text{-}X \cdots M^+ \qquad K_X = \frac{(S\text{-}X \cdots M^+)}{(S\text{-}X)(M_s^+)} \qquad [3]$$
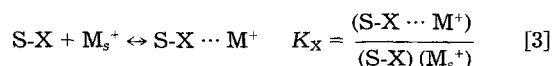
In these equations, the quantities in parentheses are ionic activities, in the case of bulk concentrations, or numbers of sites per unit surface area in the case of surface concentrations. The activity coefficients for the surface con-